Full Field Deformation Measurements During Seismic Loading of Masonry Buildings

S. Rajaram[1], P. A. Vanniamparabil[1], F. Khan[2], M. Bolhassani[2], A. Koutras[3], I. Bartoli[2], F. Moon[2], A. Hamid[2], P. Benson Shing[3], J. Tyson[4] and A. Kontsos[1,*]

[1]Department of Mechanical Engineering and Mechanics, Drexel University, Philadelphia, PA 19104
[2]Department of Civil, Architectural and Environmental Engineering, Drexel University, Philadelphia, PA 19104
[3]Department of Structural Engineering, University of California San Diego, La Jolla, CA, 92093, USA
[4]Trilion Quality Systems, Plymouth Meeting, PA 19462

Abstract

This article demonstrates the potential of the Digital Image Correlation (DIC) method to provide accurate full field deformation measurements and successfully monitor the development of damage during seismic excitation of partially grouted reinforced masonry buildings. Several earthquake load profiles were produced at the Large High Performance Outdoor Shake Table at the University of California San Diego. Using high frame rate cameras, the DIC setup was capable to measure surface deformations of the building while being at a distance of greater than 50 feet away. The accuracy of the measurements was assessed by comparison to data obtained by mounted displacement sensors. The evaluation of the recorded full field deformation data showed that the onset of damage is associated with the appearance of distinct strain localization patterns which could be tracked earlier compared to results obtained using either the displacement sensor data or by post mortem visual inspection. The research findings reported herein demonstrate for the first time to the authors' best knowledge the potential of *in situ* monitoring of actual structures under non-stationary loading profiles using optical metrology.

Keywords

Digital Image Correlation, Nondestructive Testing, Structural Health Monitoring, Concrete Masonry Walls, Shake Table

* Corresponding Author: Associate Professor, e: akontsos@coe.drexel.edu, t: (215) 895 2297

1. Introduction

The objective of this article is to investigate the potential of the Digital Image Correlation (DIC) method to provide information of importance to the structural behavior of a full scale partially grouted building undergoing seismic loading achieved at the NEES Large High Performance Outdoor Shake Table (LHPOST) at the University of California, San Diego (UCSD). This was the first time a full scale partially grouted structure was tested using the LHPOST to investigate its seismic performance as well as to provide an alternative to this type of construction [1]. The partially grouted structure was instrumented with conventional monitoring tools such as strain gages, displacement transducers and accelerometers. Data from such sensors was compared for the first time to the authors' knowledge with the application of the DIC method which provided full field optical metrology information related to deformation and damage.

Performance evaluation of modern structures subjected to seismic loading is of particular interest to structural engineering as this relates to both economically competitive design and retrofit methods. Despite the increased interest in enhancing the seismic performance and safety of critical infrastructure, considerably less attention has been given on partially grouted reinforced masonry, which can be found in almost all reinforced masonry construction in the mid-western and eastern parts of the US [2]. Specifically, although some research has been reported on the behavior of masonry under quasi static loading, only a few dynamic tests have been performed. However, dynamic characterization of masonry has a significant role in assessments of the overall structural response during seismic excitation [2, 3].

In partially grouted masonry only the location of reinforcements are grouted in contrast to fully grouted masonry in which the entire structure is grouted. Although most masonry structures in high seismic areas are restricted to be fully grouted, partially grouted masonry is favorable over

fully grouted in low seismicity areas due to its simplicity in construction and associated low cost [1]. Recent investigations have shown that masonry design provisions are unconservative and the vulnerability of this type of masonry is beyond the code estimation. Based on the available literature no conclusive assessment on the safety of partially grouted masonry buildings can be made since most of the cited research has focused only on some element of such structures [2, 3, 4]. Therefore there is a need to investigate the behavior of partially grouted masonry in a system level as well as to consider these structures under seismic loading.

Quasi-static tests performed on individual wall components have shown that the lateral load resisting mechanism found in full grouted concrete is vastly different compared to partially grouted walls. Additionally in partially grouted structures the shear strength formula used in the masonry design code underestimates the shear strength of the partially grouted components [4]. In addition, to obtain a better understanding of the mechanical behavior of masonry structures and to reduce the vulnerability of masonry a multitude of experiments are needed. However, because of the high costs of construction, the instrumentation as well as the operation of such experiments, the number of full scale tests is limited by the available resources which often leads to testing at smaller scales. Furthermore, a significant source of cost and effort is related to the instrumentation required in such experiments associated with monitoring its dynamic behavior. Consequently, the value of the research reported in this article is related to both the technical aspect of performing such large scale structural tests, as well as in the opportunity that these provided in assessing the capabilities of the DIC method when applied in such conditions.

Digital Image Correlation is a well-established optical measurement technique used to obtain full field and non-contact surface deformation [5]. DIC relies on using changes in light intensity in the captured images to define a number of digital measurement points by using primarily the

principles of photogrammetry and camera vision [6]. Typically a stochastic speckle pattern is applied using black and white paint on the surface of the testing material, component or structure [7-10]. The speckle pattern produces the necessary light contrast to produce a large number of measurement points. Images are taken before testing to provide a reference state and during the deformation process to track changes [6, 11, 12].

The DIC method was originally developed by Sutton et al. [13] whose work assisted in overcoming the limitations of similar techniques including holography, speckle photography, speckle interferometry, speckle shearing interferometry, white light speckle and moiré interferometry, while it also removed the stringent stability requirements required for the use of such interferometric methods in addition to the laborious and time consuming processing required to reduce related fringe patterns [14]. Early use of DIC focused on determining fracture mechanics parameters such as stress intensity factor in order to guide the development of analytical solutions [7] but continuously evolved to determine displacement gradients more accurately, as well as to estimate and reduce associated noise [15]. Initial work of DIC only captured two dimensional deformation until Luo et al. [16] applied stereo vision in order to obtain three dimensional measurements. The use of a stochastic speckle pattern has been investigated to understand how changes in such pattern could affect the accuracy of deformation measurements [6, 17, 18]. The advancement of DIC has been recently extended by its combined use with scanning electron microscopy (SEM) initially used for digital surface reconstruction [19], and recently extended to measure small and large deformations [20-23]. In addition using the principals of 3D DIC, digital volume correlation (DVC) applications have been reported [24-26]. Other applications include characterizing deformation mechanisms such as the ones found in metals and composites [27-32], measuring various material parameters, investigate high strain rate effects [33], high temperature

loading [34-36] and damage or fracture processes [37-39], in addition to applications were DIC data have been used to validate computational and theoretical analyses [14, 40].

The scale lengths associated with DIC measurements, as mentioned earlier, vary from the microscale [41] to large scale testing including Concrete Masonry Walls (CMW) and pre-stressed concrete structures [10, 42, 43]. For example, Vanniamparambil et al. [10] used DIC in a combined framework with other nondestructive evaluation methods to detect, monitor and quantify progressive damage in CMW subjected to cyclical lateral displacements. The authors concluded that flexural cracks were more sensitive to transversal strains while shear cracks to longitudinal strains. Similarly Ghorbani et al. [43] used DIC to measure deformation fields on full scale masonry walls and produced crack maps. Measurements of drift, diagonal deformations and interface slip between reinforced concrete columns and the masonry infill were compared to point wise sensors and showed comparable results. Related to seismic loading, research primarily has focused on seismic design that uses quasi-static lateral loading to understand performance of structures [44, 45].

The primary use of DIC in CMW applications focused on quasi static monotonic and cyclic testing with little focus on dynamic loading procedures. In order to capture the deformation process of a dynamic process a High Speed Digital Image Correlation (HSDIC) setup is generally needed. Siebert et al [46] validated HSDIC measurement data for a vibrating object capturing images at 2 kHz. Moreover, Pierron et al [47] captured full field deformation measurements of a three point bending configuration that employed a Hopkinson bar. In addition Koerber et al [33] investigated the effects of high strain rates on polymer based composite materials. An alternative to DIC, is a photogrammetry method using a 3D dynamic point tracking system. In this approach Instead of the typical speckle pattern the material or structure of interest is prepared by placing black and

white optical targets. Cameras are calibrated and positioned to determine the position of the targets relative to each other [48]. Ozbek et al [49] used this approach to monitor large wind turbines; the dynamic response of the rotor was captured using 4 cameras and 33 markers placed strategically along the turbine. Their results showed that deformations could be measured within ± 25 mm from 220 m away. Similar applications of this method have been reported for impact testing, as well as monitoring the main rotor of a helicopter in both grounded and hovering operation conditions [50-52].

The novelty of the approach presented in this article stems from implementing a HSDIC setup to monitor the mechanical behavior of a full scale partially grouted masonry wall undergoing seismic loading, for the first time to the authors' best knowledge. Full field deformation maps obtained from DIC allow clear visualization of the initiation and progression of damage during loading. By understanding the initiation of damage on a partially grouted masonry wall the identification of critical regions on the structure can be made which can assist in the effective deployment of permanent sensing devices, as well as in the optimized design of such structures.

2. Experimental Setup

The building examined was a partially grouted masonry wall assemblage considered to be the lateral resisting system of a one-story prototype structure (Figure 1A). The structure was designed for Seismic Design Category SDS C and was symmetric about the center plane along the east-west direction which corresponded to the direction of the shake-table motion. The clear height of the masonry walls was 152 in (3.86 m). The wall was constructed according to the current code provisions, the details of which conform to the current practice in that all the vertically grouted cells were separated by ungrouted masonry. Both the vertical and horizontal reinforcement had

Grade 60 No. 4 (129 sq. mm) bars. The positions of the vertical bars satisfied the code requirements in that there was vertical reinforcement of at least 0.2 sq. in (129 sq. mm) in the cross-sectional area adjacent to the openings and at wall intersections and that the maximum bar spacing did not exceed 10 ft. (3.05 m). Bond beams with horizontal reinforcement were placed at the first course above the footing and at the top course below the roof slab. The top bond beams were required to connect the roof slab to the walls with ties, however bond beams are normally not used for the first course in practice. The bottom bond beams were introduced here to provide a better performance at the base if the walls were to develop base sliding. While bond beams are required right above and below an opening according to the code, they do not need to be extended continuously along the whole wall unless they are required to resist shear. For this specimen, the intermediate bond beams were not required to resist shear, however it was deemed beneficial to tie the vertically grouted cells by bond beams at these locations so that adequate frame actions could develop if the walls were to behave similar to an infill frame, as shown in previous studies. The roof system had 8 inch thick precast hollow core planks and 4 inch reinforced concrete to achieve the desirable seismic mass. In addition, the building was instrumented with 178 strain gages on the reinforcing bars, 180 displacement transducers and 39 accelerometers (Figure 1B).

To validate the DIC measurements with conventional sensors, a comparison was made between the mounted displacement transducer SR41E that was used to measure displacement in the horizontal loading direction, shown in Figure 1. A comparison of the DIC field of view (FOV) used for the measurements reported herein and the location of SR41E is shown in Figure 1 [4]. Monochromatic images for the specific FOV shown in Figure 1 were recorded using two high speed FASTCAM SA-X cameras located approximately 50 feet (15 meters) from the building and having a relative separation of 20 feet (6 meters). The cameras were placed sufficiently far enough

from the shake table to minimize the effects of vibrations during seismic loading. A speckle pattern was applied to the front surface of the building by first applying a layer of white paint followed by painting black circles using 0.75 inch perforated sheets, as seen in Figure 1A. The diameter and separation of the black dots were computed by using tables provided by the manufacturer that take into account the camera resolution and lenses used for the given FOV. With this information at hand, the theoretical in plane displacement sensitivity was 0.003 inches with a strain sensitivity of 0.017%. In addition to the speckle pattern, large coded parkers (seen in Figure 1A) were manually placed at different locations on the wall and foundation of the building and the relative distances between them were measured prior testing to serve as fixed distances during calibration and post processing. In particular three of such coded markers were placed at the foundation of the building which for the purposes of this seismic tests was considered undeformed and therefore assisted in the relative displacement measurements reported in this investigation.

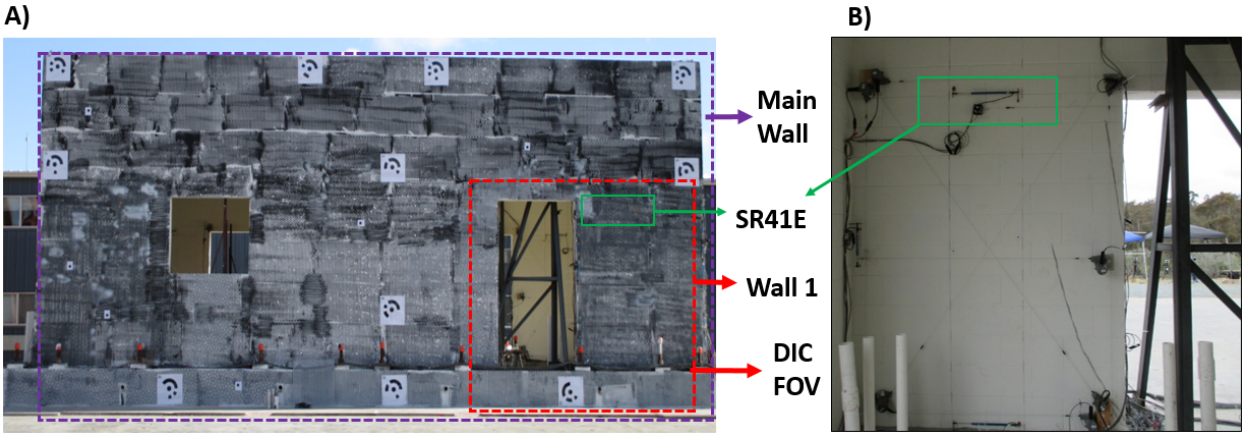

Figure 1: A) DIC FOV and approximate location of the displacement sensor (SR41E); **B)** Interior of the building showing the location of SR41E. The relative location of the DIC cameras can also be seen in the background.

All excitations applied had a duration of less than a minute and therefore the cameras chosen were set to capture an adequate number of images also based on the maximum expected vibration frequency of the building given the type of loading exerted. Specifically, images were recorded at 250Hz capturing about 21 seconds of the excitation which resulted to ~5400 images per test.

The camera lens covered a FOV of approximately 13 x 8.2 feet (4 x 2.5 meters), as shown in Figure 2A, and was calibrated using a dedicated calibration cross similar to the procedure followed previously by the authors for indoor testing of partially grouted concreted masonry walls [10]. For the calibration process, thirty seven images were captured of the cross using two cameras. The cross was physically moved to different areas, distances and angles from the wall prior testing. These images were used post mortem to create a custom calibration file that allowed images during testing to be accurately correlated. Such correlation was achieved by identifying specific points along the calibration cross from both cameras. Figure 2 contains the raw images of the cross during one instance of the process taken by the left and right camera, as well as images during the post processing that identified points along the calibration cross. For the first excitation a facet size of 33 pixels was used with a step of 10 pixels, while for the second excitation this changed to 28 and 11, respectively. Each test performed had different operating conditions due to the changing of ambient lighting and as a result the calibration process was repeated several times for consistency and validation reasons.

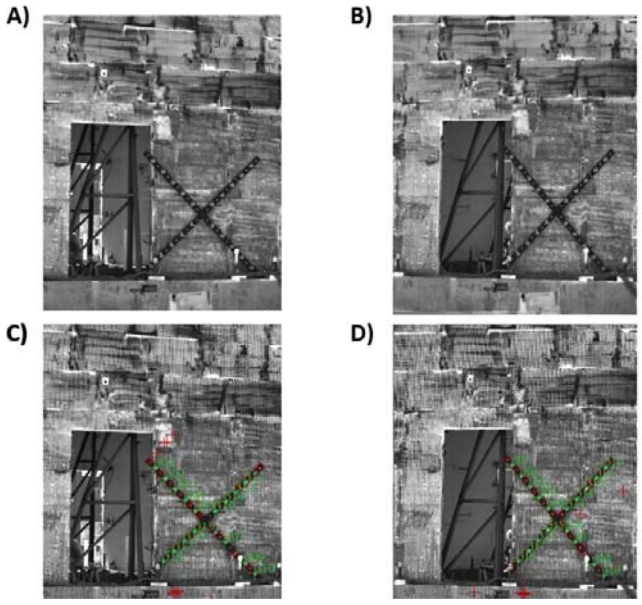

Figure 2: A) Raw image of the left camera of the calibration cross **B)** Raw image of the right camera of the calibration cross **C-D)** Identification of points along the cross of the images seen in A) and B)

The test structure was subjected to a sequence of 17 ground motions generated by the shake table. Specifically, ground motion records from the 1940 and 1979 Imperial Valley earthquakes in California, the 1985 Nahanni earthquake in Canada, and the 2011 Mineral earthquake in Virginia scaled to various intensity levels were used [5]. The actual seismic weight of the structure was 122 kips (543 kN) while the seismic weight considered in the design was 407 kips (1810 kN) based on the prototype structure. For this reason, the accelerations in the records used were scaled by a factor of 3.33 and the time scale was compressed by a factor of 0.548 to satisfy dynamic similitude requirements. After each ground motion, the structure was subjected to white-noise excitation with root-mean-square amplitude of 0.05g to determine the change of its natural frequency. The fundamental period of the undamaged structure was found to be 0.043 sec.

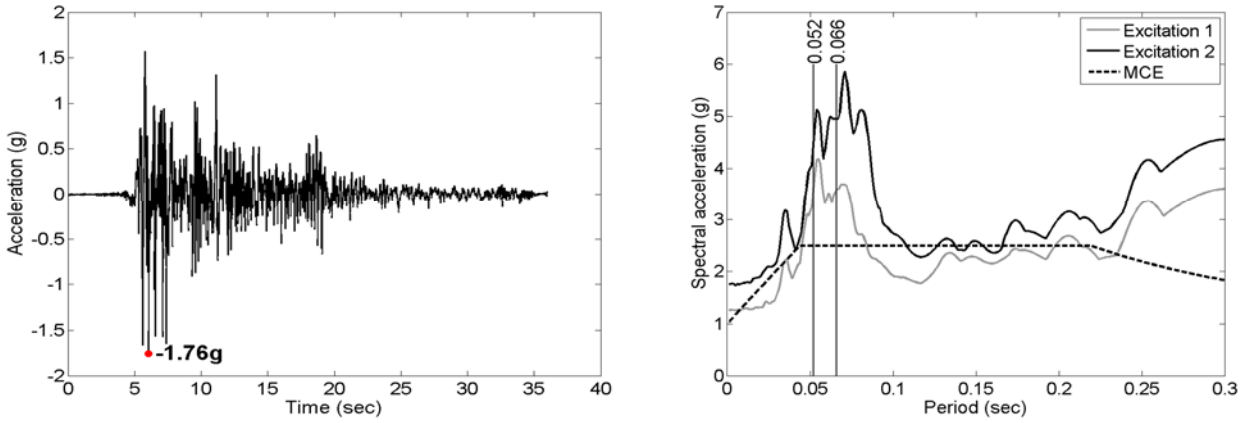

Figure 3: A) Acceleration time history of the base during excitation 2; **B)** Acceleration response spectra of excitation 1 and 2 in comparison to the MCE design spectrum.

The DIC system was employed for 12 motions, however only the last two will be discussed in this paper referred to as excitation 1 and excitation 2. Both of these excitations are scaled versions of the 1940 El Centro record. The acceleration time history of excitation 2 that was recorded at the base of the structure is shown in Figure 3A. In addition, Figure 3B illustrates the acceleration response spectrum of excitation 1 and 2 in comparison with the maximum considered earthquake

(MCE) spectrum of the design code which was 1.5 times the design earthquake spectrum of the code. Furthermore, the fundamental period of the structure measured after each excitation is shown in Figure 3B, where the fundamental period of the building before excitation 1 was equal to 0.052 sec.

3. Results and Discussion

3.1 Mounted Sensor Analysis

Excitation 1 practically did not induce any structural damage and consequently did not significantly change the natural period of the building. However, sliding occurred at the base of the structure reaching a value of 0.052 inches at the base of wall 1 and 0.091 inches at the base of the main wall. Excitation 2 was of higher intensity shifting the natural period of the structure from 0.052 to 0.066 sec, as shown in Figure 3B. Consequently, significant sliding occurred at the base of the building accompanied with the formation of shear cracks at wall 1 mainly along the height of the door. The maximum sliding recorded was smaller at the base of wall 1 (0.125 inches) compared to the main wall (0.267 inches). Figure 4 shows the time history of the pure deformation (drift) of wall 1 and the main wall which are calculated by subtracting the base sliding from the recorded displacement of the top of the wall component (by use of the SR41E displacement sensor). Based on the results in Figure 4, wall 1 experienced significantly higher deformation which lead to cracking, whereas the main wall remained practically undeformed. This could be attributed to the lower strength and larger deformation of wall 1 compared to the main wall. It should be also noted here that based on the results presented in Figure 4, and to allow further testing, concrete stoppers were installed at the ends of the main wall to prevent additional sliding.

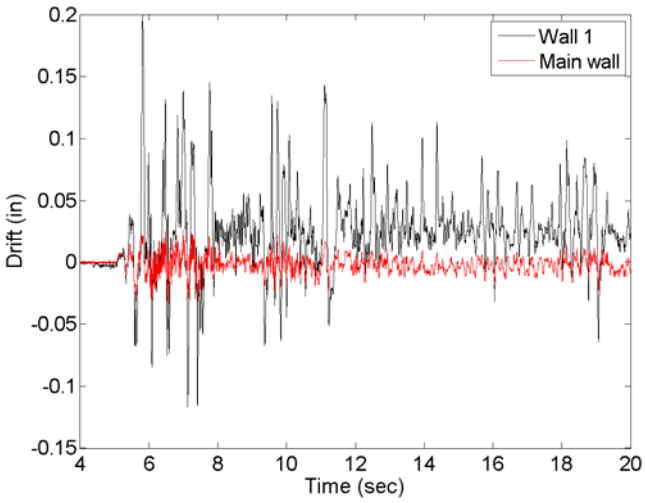

Figure 4: Time history of the drift of wall 1 and of the main wall for the excitation 2.

3.2 Comparison of DIC and displacement sensor data

The primary goal of this investigation was to capture the dynamic behavior of a concrete masonry building subjected to seismic excitation using full field deformation maps provided by the DIC method. In order to confirm the accuracy of the deformation maps, three approaches were used to validate the results: i) comparison of two different measurement tools available in DIC; ii) direct comparison of a DIC displacement measurement and a mounted displacement gage; iii) comparison of the noise floor of DIC to ensure it was within reason. Specifically, two different measurement approaches to obtain displacement values in the horizontal loading direction were used including point and virtual line gauge measurements. Point measurements are relative type measurements, in this case relative to the foundation, while virtual line gauge measurements correspond to the difference between the end points of a line placed virtually, in this case on the surface of the wall. Characteristic results for both excitations based on the application of these two methods are shown in Figure 5 and they correspond to displacements in the x-direction, which are similar to the drift reported in Figure 4 (that was solely based on the mounted displacement sensor). Overall, both methods appear to yield almost identical results.

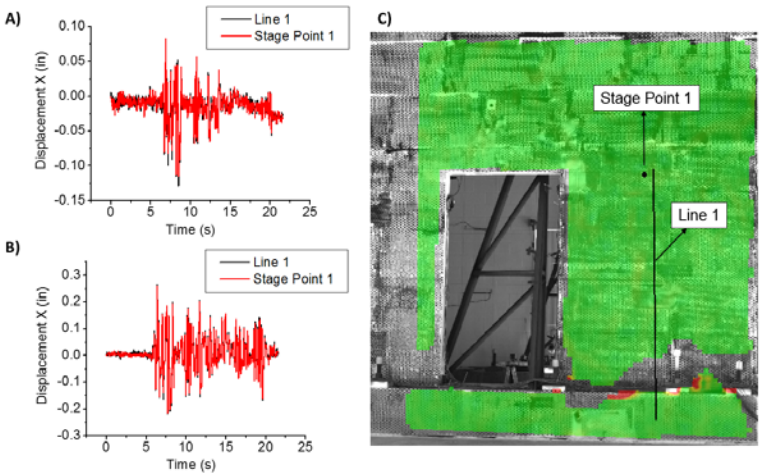

Figure 5: **A)** Comparison of displacement measurements based on Line 1 and Stage Point 1 for excitation 1; **B)** Comparison of displacement measurements based on Line 1 and Stage Point 1 for excitation 2; **C)** Visual representation of line 1 and stage point 1 on the full field displacement map overlaid on the raw image obtained by the DIC data acquisition cameras.

DIC measurements similar to the ones reported in Figure 5 were further processed to compare the differences using all 5400 images, from using half (2700 images) and from using one out every five images (1080 images). This type of comparison can be seen in Figure 6 in which three sets of DIC data computed using the virtual line gauge data are compared to displacement values measured by the SR41E sensor; this comparison reveals only minor qualitative discrepancies between the two types of data for all three sets of DIC images, which increases the confident in using non-contact, full field optical metrology for this type of structural testing.

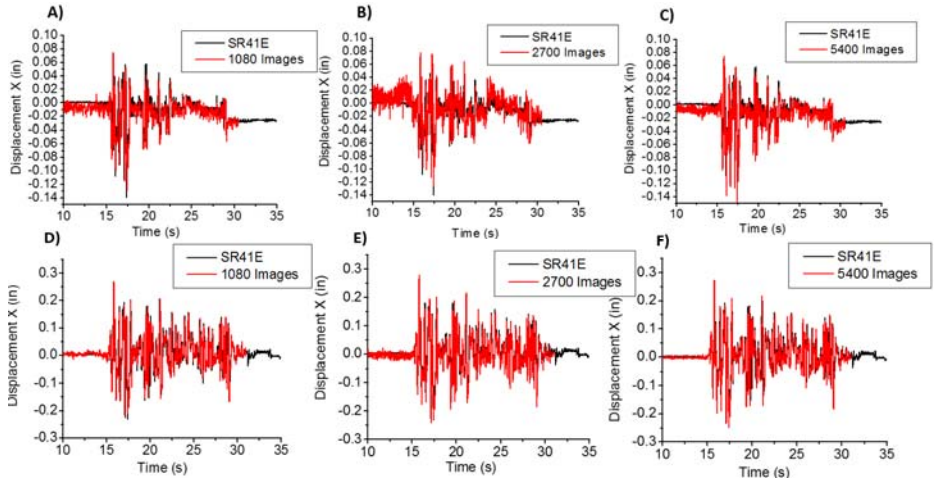

Figure 6: Comparison of displacement in the x-direction between DIC and SR41E for excitation 1 (Top) and excitation 2 (bottom) for: **A)** 1080 images, **B)** 2700 images, and **C)** 5400 images

A more quantitative way of estimating the difference between the DIC measurements using different sets of images and their comparison with the mounted sensor is reported in Table 1, in which the maximum positive displacement is reported for both excitations. Based on the results reported in Table 1, it can be concluded that the DIC method can accurately capture the dynamic behavior even during low levels of displacement caused by the much weaker first excitation.

Table 1: Comparison of DIC and SR41E

Measurement	Excitation 1 Displacement (in)	Excitation 2 Displacement (in)
SR41E	0.0709	0.270
DIC 1080 Images	0.0706	0.267
DIC 2700 Images	0.0783	0.280
DIC 5400 Images	0.0752	0.272

One of the most notable differences in the acquired DIC data stems from the associated noise. Specifically, to calculate the noise floor for these measurements, the first 5-6 seconds of both excitations during which no displacement is induced to the building were used. The noise floor created (Figure 7) was found to be between -0.02 to 0.04 inches for excitation 1 and between -0.02 to 0.02 inches for excitation 2 in the case of the 1080 images. By using, however, all the available DIC images a significant decrease in the noise floor down to approximately ∓0.006 inches was calculated which revealed a systematic bias produced from not using all images.

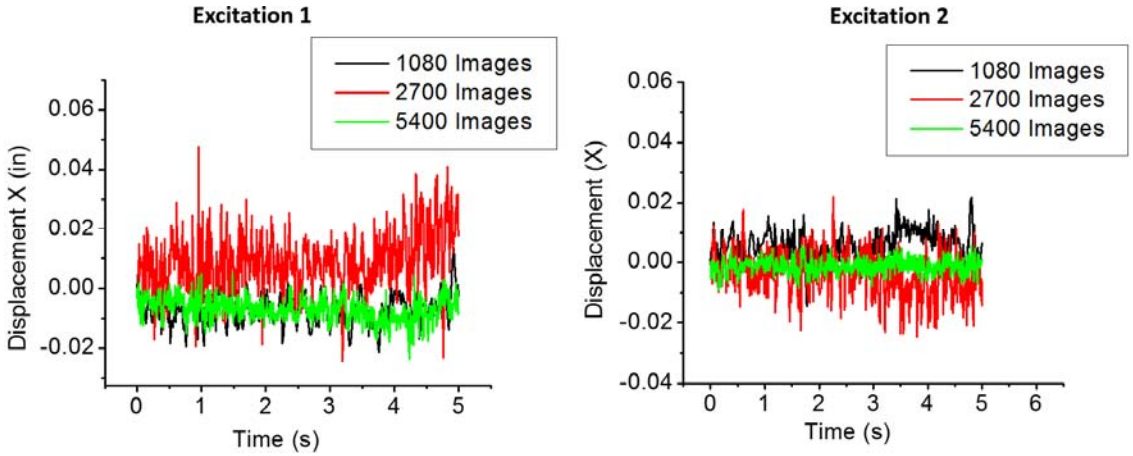

Figure 7: Computed noise floor comparison for both excitations

To further quantify the differences between the DIC and mounted sensor data a frequency response analysis was performed using both the Fast Fourier Transform (FFT) and the Short Time Fourier Transform (STFT) methods. Figure 8 clearly demonstrates that the FFT of the DIC data agrees well in terms of both the frequency and the amplitude values compared to the corresponding contact sensor data, while the STFT results show how the evolutionary frequency content is more accurately captured using the full set of 5400 images.

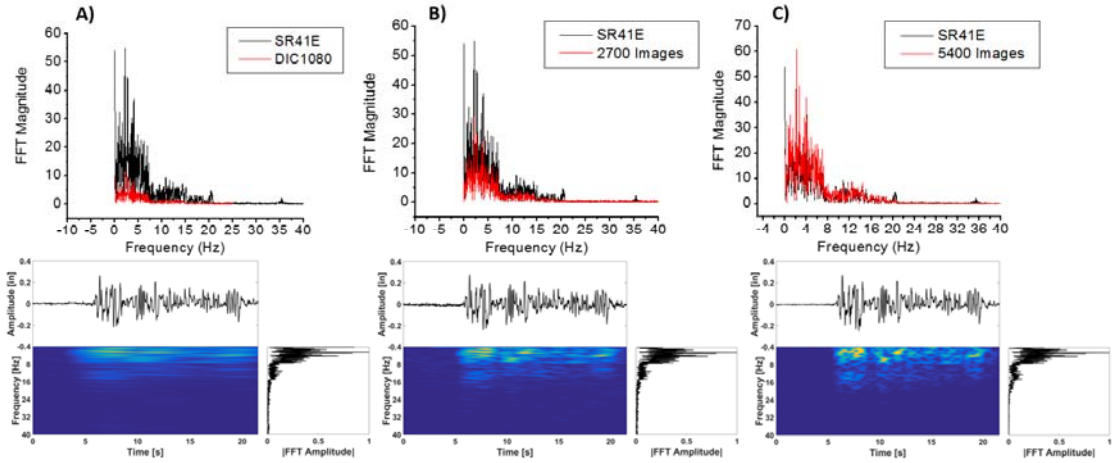

Figure 8: Comparison of DIC and SR41E frequency response using FFT analysis during excitation 2 for: **A)** 1080 Images, **B)** 2700 Images and **C)** 5400 Images. The corresponding STFT computed response of the DIC datasets is shown below each FFT comparison.

A direct comparison between the DIC dataset using all 5400 images and the SR41E sensor response in Figure 9 shows that in the same observation window the two datasets appear to have identical frequency content, which is more clearly demonstrated by plotting the corresponding FFT data for the first 5 seconds of the entire time histories. The results of this comparison can be evaluated from the perspective of the sampling frequency which was 250 Hz for the DIC method with 5400 images compared to 240 Hz for the mounted sensor. Note that this sampling rate dropped to an equivalent 50 and 125 Hz for the 1080 and 2700 images, respectively, demonstrating that a sufficiently large multiple of the peak frequency of the response needs to be accounted when capturing the transient and non-stationary characteristics of the imposed earthquake spectra.

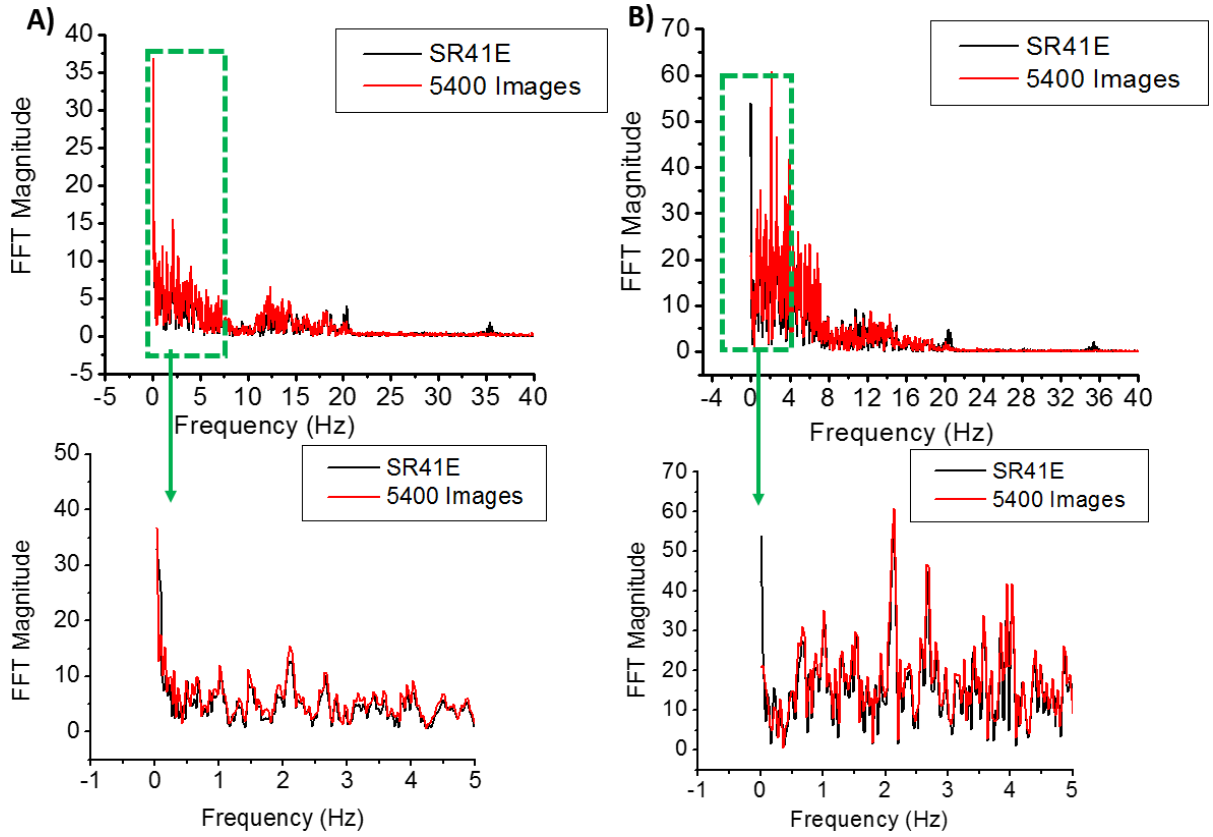

Figure 9: FFT Plots for the two excitations comparing SR41E to DIC: **A)** Excitation 1, and **B)** Excitation 2

In Figure 10, a direct comparison of the time history of the displacement amplitude for the DIC data (with 5400 images) and the mounted displacement sensor shows that the optical metrology approach succeeds in capturing both the peak values of such displacement variations, as well as the overall transient response demonstrated by the STFT results.

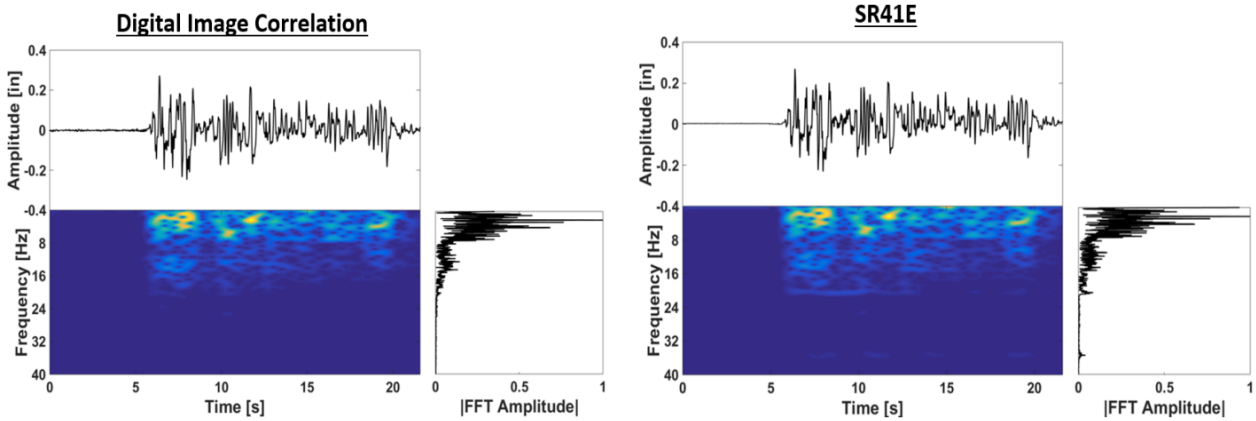

Figure 10: Comparison of STFT of DIC and SR41E during excitation 2 (Left) DIC Results (Right) SR41E Results

3.3.Damage monitoring

The validation of DIC-based displacement measurements presented in the previous sections was critical to evaluate the usefulness of strain localizations observed using the full field data and investigate their relationship to potential damage sites. As mentioned earlier, based on the mounted sensor data no shift in the fundamental period and therefore no significant damage on the building were concluded for excitation 1, which corresponds to the state-of-the-art using traditional methods of inspection.

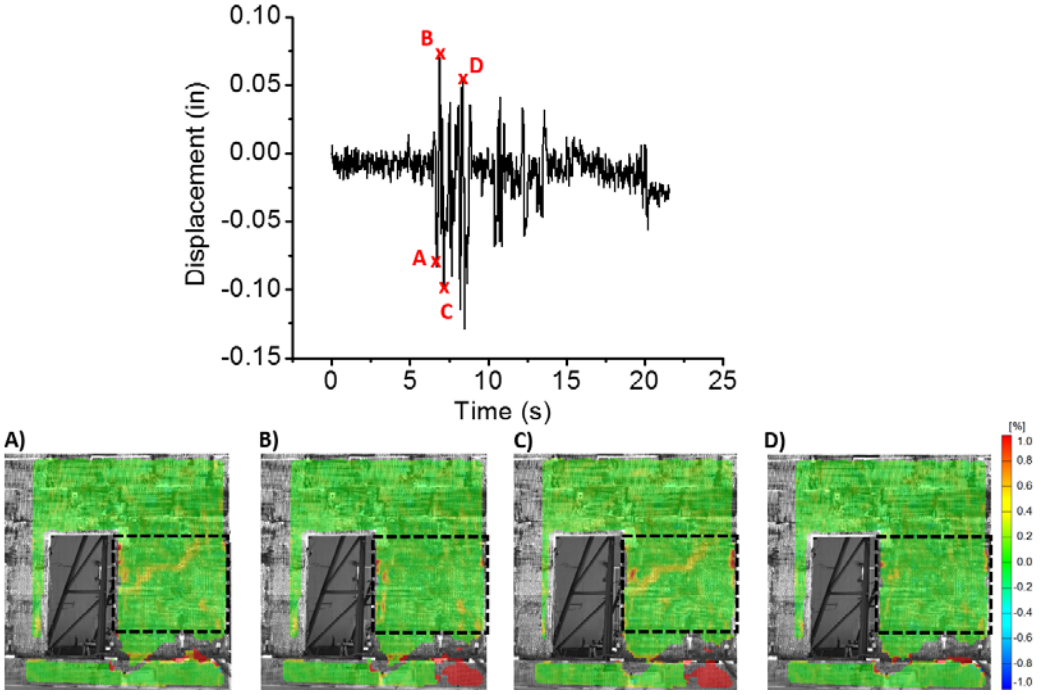

Figure 11: Full field major strain data during excitation 1 for wall 1.

The value of the DIC method in this type of structural testing could be seen precisely in this dataset in which the results shown in Figure 11 demonstrate that distinct strain localizations at wall 1 can be found in between the door and the edge of the building, the formation of which occurs only a few seconds after the initiation of the first excitation. Such strain localizations which are only possible to be found by using such full field deformation data obtained by the DIC method, could be seen to appear at four consecutive displacement extrema, demonstrating that they correspond

to actual sites where staircase patterns of cracks are occurring in agreement with previous findings by the authors in similar walls tested under cyclic loading conditions indoors [10]. Because of the lack of visible damage, such localizations can be noted as a precursors to developing damage by identifying critical regions that provide on the progressive failure pattern.

The reported strain localizations for excitation 1 become even more significant and, more importantly, they appear at the same locations during excitation 2, as shown in Figure 12, which demonstrates that the damage sites observed early in the overall structural behavior of the building are indeed occurring and lead progressively to failure. This information is critical, as it reveals the complexities of the damage process that could not only be visualized with the optical method, a fact that could assist in optimization of the placement of the mounted sensors for long term structural behavior monitoring. Such contributions could also lead to possible changes in the overall structural design and their implementation in related design codes.

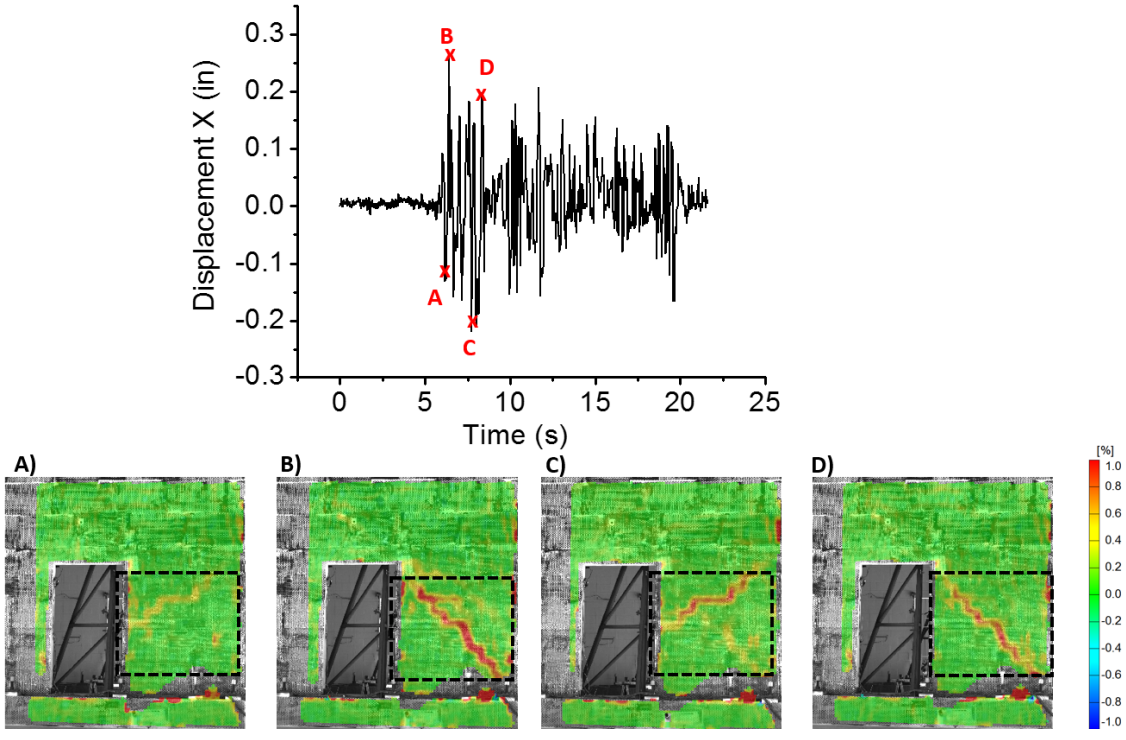

Figure 12: Full field major strain data during excitation 2 for wall 1.

In addition to observations of strain localizations, full field maps allow the computation of deformation information at several locations on the wall. Four such measurement points were placed strategically on wall 1 and the strain accumulations were quantified and compared to full field strain maps during excitation 2, as shown in Figure 13. The four points include stage point 0 on the foundation, stage point 1 at the location of SR41E, stage point 2 mid height of the doorway and stage point 3, which was chosen at a location above the doorway, as seen in Figure 13. The foundation of the building was used as a baseline for these DIC data. A comparison of the major strain time histories in Figure 13A shows that there is no distinct changes at point 1; the same holds for point 0. However, the strain data for stage point 2 show significant variations over time which correspond to time instances where strain localizations occurred as shown in Figure 13B. Similar observations can be made for stage point 3 which also corresponds to a staircase pattern of strain localization above the door.

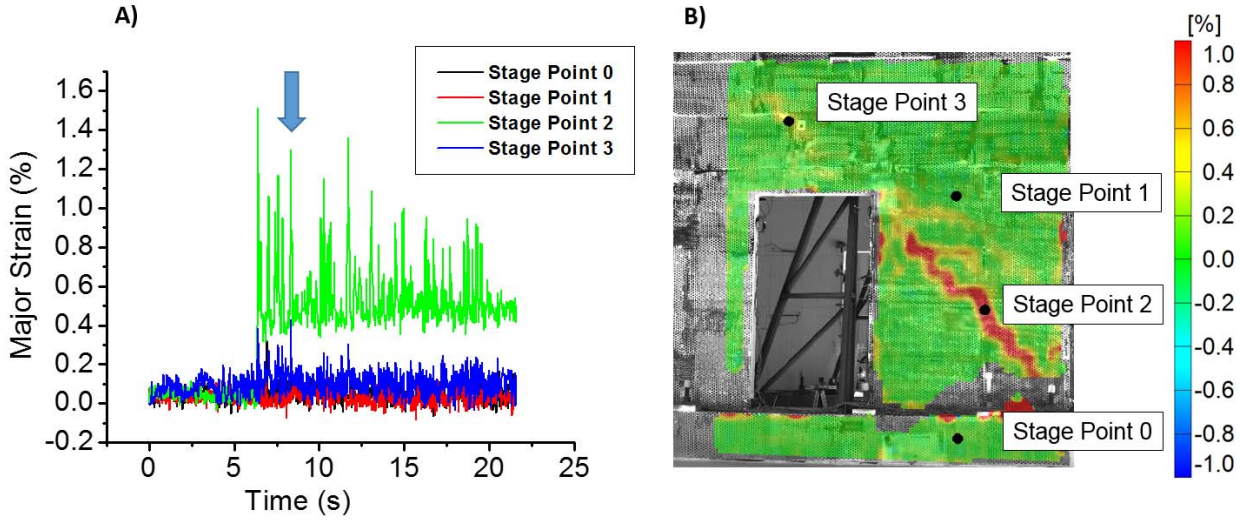

Figure 13: Major Strain at various points: **A)** Major strain time histories for each measurement point, and **B)** Location of each stage point with respect to the full field deformation data in wall 1.

The final crack pattern that was identified by post mortem visual inspection of the interior of wall 1 can be seen in Figure 14 which validates the strain localization patterns identified by the full

field strain maps and therefore demonstrates the capability of the DIC method to provide valuable information related to the structural behavior of masonry buildings subjected to seismic loading.

Figure 14: Post mortem crack pattern observation on wall 1 and comparison with characteristic full field images

4. Concluding remarks

The research findings presented in this article demonstrate that the Digital Image Correlation method, which is a non-contact, full field, optical metrology method has the potential to provide accurate deformation values at literally thousands of points on the surface of actual structures subjected to seismic loading. This is the first time that such capability is shown related to structural seismic applications to the authors' best knowledge. To validate such claims, data obtained using this optical metrology approach were compared to related measurements made by traditional contact sensors. A comparison in both the time and frequency domain revealed that full field measurements could be reliably used to compute information for structures undergoing earthquake motion. The importance of the presented approach was further shown by demonstrating early

signs of progressive failure patterns on the surface of the monitored walls which were then confirmed by post mortem visual inspection. Overall, the successful demonstration of the application of the Digital Image Correlation method in monitoring the structural behavior in seismic loading conditions creates new possibilities for the optimized placement of sensors suitable for long term structural health monitoring, as well as the improvement of assumptions related to the design of such structures and the implementation of appropriate changes in relevant codes.

Acknowledgements

The authors acknowledge the financial support received by the National Science Foundation under award No. 1208208. A. Kontsos and I. Bartoli further acknowledge the financial support received by the University of California San Diego under contract No.30037642.

References

1. Koutras, A. and P.B. Shing, *Shake-Table Tests Of Partially Grouted Reinforced Masonry Buildings.* The Masonry Society, 2015. **12th North American Masonry Conference**
2. Bolhassani, M., A.A. Hamid, and F.L. Moon, *Enhancement of lateral in-plane capacity of partially grouted concrete masonry shear walls.* Engineering Structures, 2016. **108**: p. 59-76.
3. Hamid, A., M. Bollhassani, and F. Moon, *Enhancement of Seismic Performance of Partially Grouted Reinforced Masonry Shear Walls.* 10th U.S. National Conference on Earthquake Engineering, 2014.
4. Koutras, A. and B. Shing, *Shake-Table Test of a Partially Grouted Reinforced Masonry Building with Separated Single Grouted Cells* Network for Earthquake Engineering Simulation, 2015.
5. Sutton, M.A., J.J. Orteu, and H. Schreier, *Image correlation for shape, motion and deformation measurements: basic concepts, theory and applications*. 2009: Springer Science & Business Media.
6. Lecompte, D., A. Smits, S. Bossuyt, H. Sol, J. Vantomme, D. Van Hemelrijck, and A. Habraken, *Quality assessment of speckle patterns for digital image correlation.* Optics and lasers in Engineering, 2006. **44**(11): p. 1132-1145.

7. McNeill, S.R., W.H. Peters, and M.a. Sutton, *Estimation of stress intensity factor by digital image correlation.* Engineering Fracture Mechanics, 1987. **28**(1): p. 101-112.
8. Vanniamparambil, P.A., I. Bartoli, K. Hazeli, J. Cuadra, E. Schwartz, R. Saralaya, and A. Kontsos, *An integrated structural health monitoring approach for crack growth monitoring.* Journal of Intelligent Material Systems and Structures, 2012. **23**(14): p. 1563-1573.
9. Vanniamparambil, P.A., F. Khan, K. Hazeli, J. Cuadra, E. Schwartz, A. Kontsos, and I. Bartoli, *Novel optico-acoustic nondestructive testing for wire break detection in cables.* Structural Control and Health Monitoring, 2013. **20**(11): p. 1339-1350.
10. Vanniamparambil, P.A., M. Bolhassani, R. Carmi, F. Khan, I. Bartoli, F.L. Moon, A. Hamid, and A. Kontsos, *A data fusion approach for progressive damage quantification in reinforced concrete masonry walls.* Smart Materials and Structures, 2014. **23**(1): p. 015007-015007.
11. Stoilov, G., V. Kavardzhikov, and D. Pashkouleva, *A comparative study of random patterns for digital image correlation.* Journal of Theoretical and Applied Mechanics, 2012. **42**(2): p. 55-66.
12. Mazzoleni, P., F. Matta, E. Zappa, M.A. Sutton, and A. Cigada, *Gaussian pre-filtering for uncertainty minimization in digital image correlation using numerically-designed speckle patterns.* Optics and Lasers in Engineering, 2015. **66**: p. 19-33.
13. Sutton, M., W. Wolters, W. Peters, W. Ranson, and McNeill, Sr., *Determination of displacements using an improved digital correlation method.* Image and Vision Computing, 1983. **1**(3): p. 133-139.
14. Chu, T.C., W.F. Ranson, M.a. Sutton, and W.H. Peters, *Applications of Digital Image Correlation Techniques to Experimental Mechanics.* Experimental mechanics, 1985. **25**(September): p. 232-244.
15. Sutton, M., J. Turner, H. Bruck, and T. Chae, *Full-field representation of discretely sampled surface deformation for displacement and strain analysis.* Experimental Mechanics, 1991. **31**(2): p. 168-177.
16. Luo, P.-F., Y.J. Chao, and M.A. Sutton, *Application of stereo vision to three-dimensional deformation analyses in fracture experiments.* Optical Engineering, 1994. **33**(3): p. 981-981.
17. Lecompte, D., H. Sol, J. Vantomme, and A. Habraken. *Analysis of speckle patterns for deformation measurements by digital image correlation*. in *Speckle06: Speckles, From Grains to Flowers*. 2006. International Society for Optics and Photonics.
18. Hua, T., H. Xie, S. Wang, Z. Hu, P. Chen, and Q. Zhang, *Evaluation of the quality of a speckle pattern in the digital image correlation method by mean subset fluctuation.* Optics & Laser Technology, 2011. **43**(1): p. 9-13.
19. Lockwood, W.D. and a.P. Reynolds, *Use and Verification of Digital Image Correlation for Automated 3-D Surface Characterization in the Scanning Electron Microscope.* Materials Characterization, 1999. **42**(2-3): p. 123-134.
20. Sutton, M.A., N. Li, D. Garcia, N. Cornille, J.J. Orteu, S.R. McNeill, H.W. Schreier, and X. Li, *Metrology in a scanning electron microscope: theoretical developments and experimental validation.* Measurement Science and Technology, 2006. **17**(10): p. 2613.
21. Sutton, M.A., N. Li, D. Joy, A.P. Reynolds, and X. Li, *Scanning electron microscopy for quantitative small and large deformation measurements part I: SEM imaging at magnifications from 200 to 10,000.* Experimental mechanics, 2007. **47**(6): p. 775-787.

22. Sutton, M.A., N. Li, D. Garcia, N. Cornille, J. Orteu, S. McNeill, H. Schreier, X. Li, and A.P. Reynolds, *Scanning electron microscopy for quantitative small and large deformation measurements part II: experimental validation for magnifications from 200 to 10,000.* Experimental Mechanics, 2007. **47**(6): p. 789-804.
23. Tschopp, M., B. Bartha, W. Porter, P. Murray, and S. Fairchild, *Microstructure-dependent local strain behavior in polycrystals through in-situ scanning electron microscope tensile experiments.* Metallurgical and Materials Transactions A, 2009. **40**(10): p. 2363-2368.
24. Franck, C., S. Hong, S. Maskarinec, D. Tirrell, and G. Ravichandran, *Three-dimensional full-field measurements of large deformations in soft materials using confocal microscopy and digital volume correlation.* Experimental Mechanics, 2007. **47**(3): p. 427-438.
25. Bay, B.K., T.S. Smith, D.P. Fyhrie, and M. Saad, *Digital volume correlation: three-dimensional strain mapping using X-ray tomography.* Experimental mechanics, 1999. **39**(3): p. 217-226.
26. Smith, T.S., B.K. Bay, and M.M. Rashid, *Digital volume correlation including rotational degrees of freedom during minimization.* Experimental Mechanics, 2002. **42**(3): p. 272-278.
27. Dias, G.F., M.F.S.F. de Moura, J.a.G. Chousal, and J. Xavier, *Cohesive laws of composite bonded joints under mode I loading.* Composite Structures, 2013. **106**: p. 646-652.
28. Cuadra, J., P.A. Vanniamparambil, K. Hazeli, I. Bartoli, and A. Kontsos, *Damage quantification in polymer composites using a hybrid NDT approach.* Composites Science and Technology, 2013. **83**: p. 11-21.
29. Hazeli, K., J. Cuadra, P. Vanniamparambil, R. Carmi, and A. Kontsos, *Quantification of Microstructure-Properties-Behavior Relations in Magnesium Alloys Using a Hybrid Approach.* Magnesium Technology 2014, 2014: p. 121-124.
30. Hazeli, K., J. Cuadra, P. Vanniamparambil, and A. Kontsos, *In situ identification of twin-related bands near yielding in a magnesium alloy.* Scripta Materialia, 2013. **68**(1): p. 83-86.
31. Hazeli, K., A. Sadeghi, M. Pekguleryuz, and A. Kontsos, *The effect of strontium in plasticity of magnesium alloys.* Materials Science and Engineering: A, 2013. **578**: p. 383-393.
32. Vanniamparambil, P., U. Guclu, and A. Kontsos, *Identification of Crack Initiation in Aluminum Alloys using Acoustic Emission.* Experimental Mechanics, 2015. **55**(5): p. 837-850.
33. Koerber, H., J. Xavier, and P.P. Camanho, *High strain rate characterisation of unidirectional carbon-epoxy IM7-8552 in transverse compression and in-plane shear using digital image correlation.* Mechanics of Materials, 2010. **42**(11): p. 1004-1019.
34. Chen, X., N. Xu, L. Yang, and D. Xiang, *High temperature displacement and strain measurement using a monochromatic light illuminated stereo digital image correlation system.* Measurement Science and Technology, 2012. **23**(12): p. 125603-125603.
35. Pan, B., D. Wu, Z. Wang, and Y. Xia, *High-temperature digital image correlation method for full-field deformation measurement at 1200 °C.* Measurement Science and Technology, 2011. **22**(1): p. 015701-015701.
36. Pan, B., D. Wu, and Y. Xia, *High-temperature deformation field measurement by combining transient aerodynamic heating simulation system and reliability-guided digital image correlation.* Optics and Lasers in Engineering, 2010. **48**(9): p. 841-848.

37. Skarżyński, Ł. and J. Tejchman, *Experimental Investigations of Fracture Process Using DIC in Plain and Reinforced Concrete Beams under Bending.* Strain, 2013. **49**(6): p. 521-543.
38. Tracy, J., A. Waas, and S. Daly, *A New Experimental Approach for In Situ Damage Assessment in Fibrous Ceramic Matrix Composites at High Temperature.* Journal of the American Ceramic Society, 2015. **9**(35116): p. n/a-n/a.
39. Zhang, H., D. Fu, H. Song, Y. Kang, G. Huang, G. Qi, and J. Li, *Damage and Fracture Investigation of Three-Point Bending Notched Sandstone Beams by DIC and AE Techniques.* Rock Mechanics and Rock Engineering, 2014(Dic).
40. Pan, B., K. Qian, H. Xie, and A. Asundi, *Two-dimensional digital image correlation for in-plane displacement and strain measurement: a review.* Measurement Science and Technology, 2009. **20**(6): p. 062001-062001.
41. Berfield, T.a., J.K. Patel, R.G. Shimmin, P.V. Braun, J. Lambros, and N.R. Sottos, *Micro- and Nanoscale Deformation Measurement of Surface and Internal Planes via Digital Image Correlation.* Experimental Mechanics, 2007. **47**(1): p. 51-62.
42. Gencturk, B., K. Hossain, A. Kapadia, E. Labib, and Y.-L. Mo, *Use of digital image correlation technique in full-scale testing of prestressed concrete structures.* Measurement, 2014. **47**: p. 505-515.
43. Ghorbani, R., F. Matta, and M.a. Sutton, *Full-Field Deformation Measurement and Crack Mapping on Confined Masonry Walls Using Digital Image Correlation.* Experimental Mechanics, 2014.
44. Smith, B.J., Y.C. Kurama, and M.J. McGinnis, *Design and Measured Behavior of a Hybrid Precast Concrete Wall Specimen for Seismic Regions.* Journal of Structural Engineering, 2011. **137**(10): p. 1052-1062.
45. Banting, B.R. and W.W. El-Dakhakni, *Seismic Design Parameters for Special Masonry Structural Walls Detailed with Confined Boundary Elements.* ASCE Journal of Structural Engineering, 2007. **1**(June): p. 1-18.
46. Siebert, T., T. Becker, K. Spiltthof, I. Neumann, and R. Krupka, *High-speed digital image correlation: error estimations and applications.* Optical Engineering, 2007. **46**(May 2007): p. 051004-051004.
47. Pierron, F., M.a. Sutton, and V. Tiwari, *Ultra High Speed DIC and Virtual Fields Method Analysis of a Three Point Bending Impact Test on an Aluminium Bar.* Experimental Mechanics, 2011. **51**: p. 537-563.
48. Carr, J., J. Baqersad, C. Niezrecki, and P. Avitabile, *Full Field Dynamic Strain on Wind Turbine Blade Using Digital Image Correlation Techniques and Limited Sets of Measured Data from Photogrammetric Targets.* Experimental Techniques, Society for Experimental Mechanics, 2014: p. 1-13.
49. Ozbek, M., D.J. Rixen, O. Erne, and G. Sanow, *Feasibility of monitoring large wind turbines using photogrammetry.* Energy, 2010. **35**(12): p. 4802-4811.
50. Lundstrom, T., J. Baqersad, and C. Niezrecki, *Monitoring the Dynamics of a Helicopter Main Rotor With High-Speed Stereophotogrammetry.* Experimental Techniques, 2015: p. n/a-n/a.
51. Pereira, J.M., D.M. Revilock, C.R. Ruggeri, W.C. Emmerling, and D.J. Altobelli, *Ballistic Impact Testing of Aluminum 2024 and Titanium 6Al-4V for Material Model Development.* 2014. **27**(3): p. 456-465.

52. Seidt, J.D., J. Michael Pereira, A. Gilat, D.M. Revilock, and K. Nandwana, *Ballistic impact of anisotropic 2024 aluminum sheet and plate.* International Journal of Impact Engineering, 2013. **62**: p. 27-34.